High Oxidation States

DOI: 10.1002/anie.200902733

Formation and Characterization of the Iridium Tetroxide Molecule with Iridium in the Oxidation State +VIII**

Yu Gong, Mingfei Zhou, Martin Kaupp, and Sebastian Riedel**

Dedicated to Professor Pekka Pyykkö

The highest known oxidation state of any chemical element is +VIII. Apart from some xenon compounds, this oxidation state is represented by the well-characterized RuO_4 and OsO_4 transition-metal complexes[1–6] (and by some derivatives of the latter). In this case, the maximum oxidation state coincides with the group number 8 and thus with the number of valence electrons. For the 5d transition elements to the right of Os in the periodic table, an oxidation state equal to the group number is not reached anymore. Quantum-chemical studies had predicted a linear decrease[7] of the highest accessible fluoride oxidation states from Ir^{VII} towards Hg^{IV}, and the latter could recently be experimentally identified as HgF_4 by low-temperature matrix-isolation spectroscopy.[8] However, higher oxidation states of iridium than +VI had not yet been confirmed experimentally. Iridium(VI) is represented by IrF_6 and by a number of perovskites containing the $[IrO_6]^{6-}$ ion.[9] An early suggestion of the gas-phase preparation of IrO_4 with iridium in the oxidation state +VIII has long been disproved by equilibrium measurements of the gas phase over Ir or IrO_2 solids, which were assigned the composition IrO_3 (without structural proof).[10–12]

A matrix-isolation infrared spectroscopic study on the reaction products from co-deposition of laser-ablated iridium atoms and dioxygen provided evidence for the formation of a side-on bonded iridium dioxide peroxide complex, whereas a proper iridium(VIII) tetroxide was not identified.[13] Recent quantum-chemical calculations on iridium fluoride and oxide-fluoride complexes suggested the existence of the +VIII and +IX oxidation states to be unlikely, and Ir^{VII} was indicated to be the highest realistic oxidation state in these cases.[7] However, herein we report the production and identification of the genuine iridium(VIII) tetroxide molecule at low temperature in solid neon, argon, and krypton.

The iridium oxide species were prepared by co-deposition of laser-evaporated iridium atoms with O_2/Ng (Ng = Ne, Ar, Kr) mixtures onto a CsI window at 4 K (Ne) or 6 K (Ar and Kr) as previously described.[14] Infrared spectra were recorded on a Bruker IFS 66 V spectrometer at 0.5 cm^{-1} resolution using a liquid-nitrogen-cooled mercury cadmium telluride (MCT) detector. The infrared spectra in the O-O and Ir=O stretching frequency region from co-deposition of laser-evaporated Ir atoms with 0.1% O_2 in argon are shown in Figure 1.

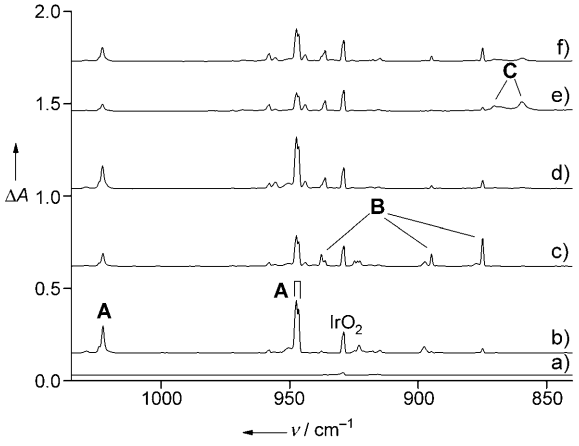

Figure 1. Infrared spectra in the 1035–840 cm^{-1} region from co-deposition of laser-evaporated iridium atoms with 0.1% O_2 in argon: a) after 1.5 h of sample deposition at 6 K; b) after annealing to 30 K in dark; 10 scans; c) as for (b), but with 370 scans; d) after 10 min of $\lambda > 850$ nm irradiation; 10 scans; e) after 15 min of $\lambda > 500$ nm irradiation; 10 scans; f) after 10 min of $\lambda > 300$ nm irradiation; 10 scans. Labels **A**, **B**, and **C** denote the absorptions of the $[(\eta^1\text{-}O_2)IrO_2]$, $[(\eta^2\text{-}O_2)IrO_2]$, and IrO_4 species, respectively.

After 1.5 h of sample deposition, no product absorption bonds were observed in the spectrum except for the weak absorption bands at 929.0 and 915.7 cm^{-1} for the neutral and anionic linear dioxide, which have previously been identified.[13,15] When the as-deposited sample was annealed to

[*] Y. Gong, Prof. Dr. M. F. Zhou
Department of Chemistry
Shanghai Key Laboratory of Molecular Catalysts and Innovative Materials
Advanced Materials Laboratory, Fudan University
Shanghai 200433 (China)
Fax: (+86) 21-6564-3532
E-mail: mfzhou@fudan.edu.cn
Dr. S. Riedel
Institut für Anorganische und Analytische Chemie
Albert-Ludwigs Universität Freiburg
Albertstrasse 21, 79104 Freiburg i. Br. (Germany)
Fax: (+49) 761-203-6001
E-mail: sriedel@psichem.de
Prof. Dr. M. Kaupp
Institut für Anorganische Chemie der Universität Würzburg
Am Hubland, 97074 Würzburg (Germany)

[**] We are grateful to D. Himmel for stimulating discussions. This work was supported by the National Basic Research Program of China (2007CB815203) and the National Natural Science Foundation of China (20773030). S.R. thanks the Alexander von Humboldt Foundation and the DFG for research fellowships.

Supporting information for this article is available on the WWW under http://dx.doi.org/10.1002/anie.200902733.

 © 2009 Wiley-VCH Verlag GmbH & Co. KGaA, Weinheim

30 K, the IrO_2 absorption increased and a group of new absorption bands formed at 2026.3, 1966.5, 1885.5, 1022.6, 947.4, and 946.6 cm^{-1} (labeled **A** in Figure 1, the spectra in the high-frequency region are shown in Figure S1 in the Supporting Information). These absorptions decayed quickly with increasing sample scan times (Figure 1, trace c), indicating that the carriers for these bands are unstable toward infrared irradiation from the source of the spectrometer (7500–370 cm^{-1}). With the decrease of group **A** absorption bands, a second group of absorption bands at 1803.4, 937.7, 894.8, 874.9, 547.9, and 517.8 cm^{-1} (labeled **B** in Figure 1) were produced. Irradiation with light from a tungsten lamp with a $\lambda > 850$ nm long-wavelength pass filter reduced group **B** absorption bands and recovered group **A** absorption bands (Figure 1, trace d). Further irradiation from the tungsten lamp with a $\lambda > 500$ nm long-wavelength pass filter decreased both group **A** and **B** absorption bands. In concert, two broad absorption bands at 870.5 and 859.5 cm^{-1} (labeled **C** in Figure 1) were produced at the expense of group **A** and **B** absorption bands. The group **C** absorption bands decreased and group **A** and **B** absorption bands recovered under irradiation with light from a mercury arc lamp with a $\lambda >$ 300 nm long-wavelength pass filter ($300 < \lambda < 580$ nm). The experiments were repeated under the same conditions using the $^{18}O_2$, $^{16}O_2 + {}^{18}O_2$, and $^{16}O_2 + {}^{16}O^{18}O + {}^{18}O_2$ samples to help product identification on the basis of isotopic shifts and absorption splittings. The isotopic spectra in selected regions are shown in Figures S2 and S3, and the product absorptions are listed in Table S1 (in the Supporting Information).

Similar experiments were performed with laser-evaporated iridium and O_2 in excess neon and krypton. The spectra are shown in Figures S4–S6 in the Supporting Information. They are much the same as those illustrated in Figure 1. The product absorption bands in solid neon and krypton are less than 10 cm^{-1} blue- or red-shifted from those of in solid argon (Table S2 in the Supporting Information). The small argon-to-neon or -krypton matrix shifts observed for the product absorption bands verify that there is no unusual matrix effect on these guest molecules.[16]

The absorption bands at 1803.4, 937.7, 874.9, 547.9, and 517.8 cm^{-1} of group **B** were attributed to the side-on bonded $[(\eta^2\text{-}O_2)IrO_2]$ complex in the previous report.[13] The 937.7 and 874.9 cm^{-1} absorption bands are due to the symmetric and antisymmetric O-Ir-O stretching vibrations (Table 1). Along with these absorption bands, an additional absorption band at 894.8 cm^{-1} showed identical behavior after irradiation and annealing. The isotopic frequency ratio of 1.0591 is appropriate for the O-O stretching vibration of the $[(\eta^2\text{-}O_2)IrO_2]$ complex. The observed O-O stretching frequency falls in the range expected for peroxides,[17–19] and, hence, the $[(\eta^2\text{-}O_2)IrO_2]$ complex can be regarded as $[(IrO_2)^{2+}(O_2^{2-})]$, a side-on bonded iridium dioxide peroxide complex.

The group **A** absorption bands are photoreversible with the $[(\eta^2\text{-}O_2)IrO_2]$ absorption bands (group **B**), which suggests that the species responsible for group **A** absorption bands is a structural isomer of $[(\eta^2\text{-}O_2)IrO_2]$. These absorption bands are assigned to different vibrational modes of the $[(\eta^1\text{-}O_2)IrO_2]$ complex (Table 1). The partially overlapping 947.4 and 946.6 cm^{-1} absorption bands are due to the antisymmetric and symmetric O-Ir-O stretching vibrations. The 1022.6 cm^{-1} absorption peak shifted to 965.9 cm^{-1} with $^{18}O_2$. The band position and isotopic frequency ratio (1.0587) are appropriate for an O-O stretching vibration. The observation of overtone and combination modes above 1800 cm^{-1} (Table 1) lends additional support to the assignment. The band position of the O-O stretching vibration indicates that the $[(\eta^1\text{-}O_2)IrO_2]$ complex is an end-on bonded iridium dioxide superoxide complex. Similar end-on bonded metal dioxide superoxide complexes have been reported for iron and cobalt.[20,21]

The group **C** absorption bands at 870.5 and 859.5 cm^{-1} appeared only under $\lambda > 500$ nm irradiation at the expense of group **A** and **B** absorption bands. It was found that group **C** absorption bands are also photoreversible with the $[(\eta^1\text{-}O_2)IrO_2]$ and $[(\eta^2\text{-}O_2)IrO_2]$ absorption bands, suggesting that the species responsible for group **C** absorption bands is a third isomer with IrO_4 stoichiometry. The band positions and isotopic frequency ratios (1.0543 and 1.0551) indicate that these two absorption bands are due to antisymmetric O=Ir=O stretching vibrations. No other vibrational modes were

Table 1: Observed and computed vibrational frequencies of the IrO_4 isomers.

	Expt.[a]	ν[b] [cm^{-1}]	I [km mol^{-1}]	Mode
	2026.3			2ν (O-O str.)
	1966.5			O-O str. + O-Ir-O sym. str.
	1885.5			sym. + antisym. O-Ir-O str.
$[(\eta^1\text{-}O_2)IrO_2]$ (**A**)	1022.6	1022	146	O-O str.
		1113	*84*	
	947.4	971	50	antisym. O-Ir-O str.
		999	*211*	
	946.6	959	160	sym. O-Ir-O str.
		1024	*67*	
	1803.4			sym. + antisym. O-Ir-O str.
	937.7	952	81	sym. O-Ir-O str.
		997	*80*	
	894.8	*950*	2	O-O str.
		992	*2*	
$[(\eta^2\text{-}O_2)IrO_2]$ (**B**)	874.9	872	123	antisym. O-Ir-O str.
		899	*135*	
	547.9	568	7	Ir-O_2 str.
		578	*9*	
	517.8	505	3	Ir-O_2 str.
		532	*3*	
		908	–	sym. O-Ir-O str.
		955	–	
		(919)	–	
IrO_4 (**C**)	870.5[c]	897	2×76	antisym. O-Ir-O str.
		936	*2×97*	
		(931)	–	
	859.5[c]	865	81	antisym. O-Ir-O str.
		900	*105*	
		(906)	–	

[a] Experimental results in an argon matrix. [b] BP86, B3LYP, and CCSD(T) computations at harmonic level (only absorption peaks above 400 cm^{-1} are listed). B3LYP values in italics and CCSD(T) values in parentheses. [c] The IrO_4 modes are observed at 869.0 and 859.2 cm^{-1} in neon and at 868.1 and 858.2 cm^{-1} in krypton.

 © 2009 Wiley-VCH Verlag GmbH & Co. KGaA, Weinheim

observed, which implies that species **C** involves only terminal Ir=O bonds. The experimental isotopic shifts of 44.8 and 44.9 cm^{-1} and CCSD(T) calculated results of 47.8 and 47.9 cm^{-1} for iridium tetroxide agree excellently (Table S6 in the Supporting Information and below). We thus assign the 870.5 and 859.5 cm^{-1} absorption bands to a genuine iridium tetroxide molecule (Table 1). Anharmonic corrections at DFT level improve the agreement between computed (BP86: 885, 857 cm^{-1}; B3LYP: 923, 892 cm^{-1}) and measured (Ar matrix: 870.5, 859.5 cm^{-1}) frequencies (see also Table S11 in the Supporting Information). The tetrahedral OsO_4 molecule has only one IR-active Os=O stretching vibration, which was observed at 956.2 cm^{-1} in solid argon.[22]

To validate the experimental assignment and to understand the conditions for the formation of IrO_4, further quantum-chemical calculations were performed on the three structural isomers of IrO_4 and, for comparison, on the corresponding OsO_4 isomers (Figure S7 in the Supporting Information gives the B3LYP-optimized structures of the IrO_4 isomers). As can be seen from Table 1, apart from a systematic overestimate of the frequency, the computed stretching frequencies support the spectra assignments. Structurally, species **A** is confirmed to be the end-on bonded superoxide complex $[(\eta^1\text{-}O_2)IrO_2]$ with C_s symmetry and electron configuration $^2A''$. Species **B**, the side-on bonded peroxido complex $[(\eta^2\text{-}O_2)IrO_2]$, exhibits C_{2v} symmetry with electron configuration $^2A_2$, with a reasonable O-O bond length of 145.1 pm at CCSD(T) level (Table S3 in the Supporting Information, cf. experimental value of 147.5 pm for H_2O_2[23]).

The third isomer is a true tetroxide with four terminal Ir–O bonds (species **C**). Because of its d^1 configuration, IrO_4 exhibits moderate Jahn–Teller distortion from a regular tetrahedron to D_{2d} symmetry ($^2A_1$ ground state; Table S3 in the Supporting Information). Closer analysis confirms clearly the assignment of a formal oxidation state Ir^{VIII} to this complex.

The computed 0 K energetics (B3LYP level) of these three isomers are provided in Figure 2, including barriers for interconversion between them (results at other levels, including CCSD(T), are given in Table S5 in the Supporting Information). To put these data into perspective, the same information is included also for the much better known OsO_4.[22] Importantly, the true tetroxide is the lowest-energy minimum not only for OsO_4 but also for IrO_4, although the potential-energy diagram is much more shallow for the latter. Although the other two IrO_4 isomers come to within less than 100 kJ mol^{-1} of the tetroxide (with activation barriers on the order of about 125 kJ mol^{-1}), the corresponding OsO_4 isomers are extremely unstable, with much larger barriers.

At the indicated conditions, IrO_4 is stable with respect to unimolecular elimination of O_2. That is, ΔH at 0 K for the reaction $IrO_{4(g)} \rightarrow IrO_{2(g)} + O_{2(g)}$ is computed to be on the order of 150–200 kJ mol^{-1} at CCSD(T) level (with more positive values for larger basis sets, Table S4 in the Supporting Information). Of course the corresponding reaction is even more endothermic (+576.5 kJ mol^{-1} at CCSD(T)/aug-cc-pVTZ level) for OsO_4. These results are on the one hand consistent with the existence of iridium tetroxide under the low-temperature inert-gas matrix conditions of the present work but on the other hand confirm the much larger stability of osmium(VIII) tetroxide.

Together with some additional experimental data (see Table S6 in the Supporting Information), these results enable us to set up Born–Haber cycles aimed at estimating the stabilities in the bulk condensed phase (Scheme 1). To get the $\Delta H°$, $\Delta S°$, and $\Delta G°$ values for the reactions $MO_{2(s)} + O_{2(g)} \rightarrow MO_{4(s)}$ (see also data given in Table S6), the condensation energy $IrO_{4(g)} \rightarrow IrO_{4(s)}$ has been set equal to the known (low) value for OsO_4. This assumption is confirmed by further calculations (B3LYP) of dimer complexes such as $[O_3IrOOIrO_3]$ or $[O_2Ir(OO)_2IrO_2]$, which are all unbound with respect to two IrO_4 molecules (see Figure S8 in the Supporting Information), and is consistent with the assumed monomeric nature of IrO_4. The Born–Haber cycles of Scheme 1 indicate that condensed-phase $IrO_{4(s)}$ at room

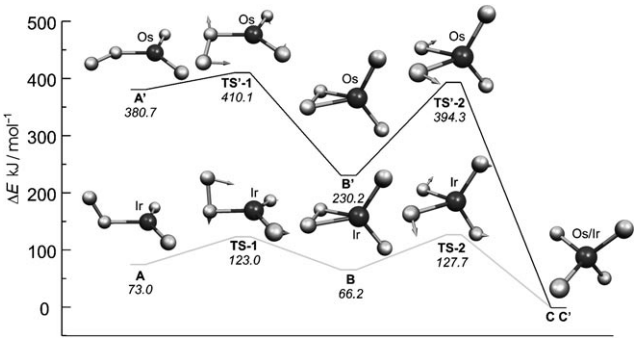

Figure 2. Computed potential-energy diagram (B3LYP results) of the isomers of MO_4 (M = Ir, Os). The bottom line shows M = Ir, the upper line M = Os; values in italics are energies in kJ mol^{-1} relative to the most stable tetrahedral isomer MO_4 (see Table S4 in the Supporting Information). Arrows on the transition state structures indicate the directions of the force constants of the imaginary mode (arrow scale factor 0.2)

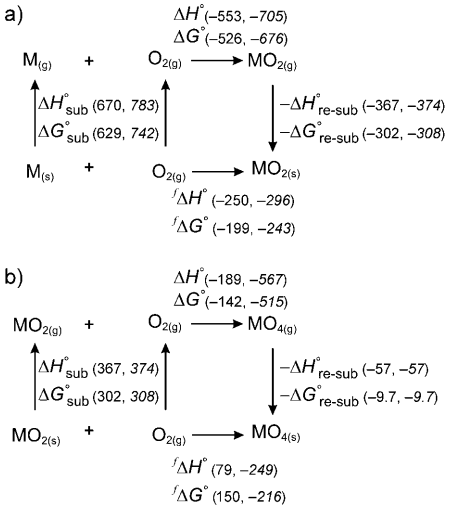

Scheme 1. Representative thermochemical (Born–Haber) cycles at 298.15 K for the di- and tetroxides. Values in parentheses are in kJ mol^{-1}; Roman text style represents iridium and italics represents osmium.

 © 2009 Wiley-VCH Verlag GmbH & Co. KGaA, Weinheim

temperature is unstable with respect to $IrO_{2(s)} + O_{2(g)}$, whereas $OsO_{4(s)}$ is stable with respect to the analogous reaction. This in turn may be traced back to the quantitatively different energy values for the gas-phase elimination reaction $MO_{2(g)} + O_{2(g)} \rightarrow MO_{4(g)}$, (Table S4). That is, IrO_4 is sufficiently stable to be isolated under the present matrix-isolation conditions but will not survive as a bulk solid at higher temperatures (it will probably not even be metastable; see Figure 2).

In conclusion, matrix-isolation experiments in neon, argon, and krypton matrices clearly show IR absorptions that are consistent with the formation of a true iridium tetroxide ($Ir^{VIII}O_4$) with d^1 configuration. This result is supported by accurate quantum-chemical calculations, which indicate the tetroxide to be the most stable isomer, albeit with a more shallow potential-energy surface for rearrangements than that computed for the analogous tetroxide OsO_4. The construction of Born–Haber cycles shows why IrO_4 could not be observed as a bulk solid under conditions for which OsO_4 is known. IrO_4 is much less stable than OsO_4 under comparable conditions but may be stabilized in low-temperature matrices. As the Jahn–Teller-distorted tetrahedral IrO_4 is undoubtedly a proper d^1 system (see, for example, the spin-density distribution in Figure S9 in the Supporting Information), the new oxidation state Ir^{VIII} has thus been established.

Experimental Section

Computational methods: Calculations were performed at various levels of density functional theory (DFT) and at ab initio levels up to CCSD(T). DFT calculations were performed with the Gaussian03[24] program package and the analytical gradient methods implemented therein. The gradient-corrected BPW91[25,26] and BP86 functionals and the hybrid functional B3LYP (based on the work of Becke)[27] were used. The selection of B3LYP was based on its excellent performance for the redox thermochemistry of transition-metal systems in high oxidation states.[9] GGA functionals (BPW91, BP86) tend to overestimate the stability of the higher oxidation states,[13] as do Møller–Plesset perturbation (MP2) calculations. BP86 vibrational frequencies, which agree even better with experiment than the B3LYP results, are also given in Tables 1 and S11 (in the Supporting Information). Anharmonic corrections were calculated at DFT (BP86 and B3LYP/aug-cc-pVTZ) levels using the Gaussian03[24] program package. The MP2 and coupled-cluster calculations with single and double substitutions (CCSD), as well as with the inclusion of perturbative triple excitations [CCSD(T) level], were carried out with the MOLPRO 2006 program package.[28] Coupled-cluster frequencies were obtained by numerical differentiation of analytical first derivatives. All species were fully optimized at a given computational level. Coupled-cluster single-point energies were also computed at various B3LYP-optimized structures.

Scalar relativistic effects for iridium and osmium were included by a quasirelativistic energy-adjusted, small-core pseudopotential (effective-core potential, ECP).[29] The corresponding (8s7p6d)/[6s5p3d] valence basis set was augmented by one f-type polarization function (Ir $\alpha_f = 0.938$, Os $\alpha_f = 0.886$).[30] For comparison, in some calculations, the valence basis set was also augmented by 2f and 1g-type polarization functions ($\alpha_f = 0.395$, 1.189, and $\alpha_g = 0.982$).[31] The oxygen atoms were described by a Dunning aug-cc-pVTZ basis set.[32] Subsequent single-point energy calculations at MP2 and coupled-cluster CCSD and CCSD(T) levels used also larger aug-cc-pVnZ (n = Q, 5) oxygen basis sets.

Basis-set superposition errors (BSSE) were neglected because of our experience of only marginal BSSE effects for the basis-set sizes used.[7,33–35] Zero-point vibrational energy (ZPE) corrections were computed at DFT and ab initio levels up to CCSD(T). Spin-orbit (SO) coupling was neglected on the basis of our experience for mercury fluorides[36] and on results for gold complexes.[37] SO effects are expected to influence reaction energies involving only closed-shell species negligibly. In the case of the open-shell species, we cannot exclude completely some influence of SO effects as it is shown in reference [7] for iridium species. However, as the SO effects derive mainly from the 5d shell, they are expected to be only moderate.

Received: May 22, 2009
Published online: July 11, 2009

Keywords: density functional calculations · dioxygen ligands · high oxidation states · iridium · matrix isolation

[1] O. Ruff, E. Vidic, *Z. Anorg. Allg. Chem.* **1924**, *136*, 49.
[2] M. Pley, M. S. Wickleder, *J. Solid State Chem.* **2005**, *178*, 3206.
[3] A. J. Bailey, M. G. Bhowon, W. P. Griffith, A. G. F. Shoair, A. J. P. White, D. J. Williams, *J. Chem. Soc. Dalton Trans.* **1997**, 3245.
[4] H. Kunkely, A. Vogler, *Inorg. Chem. Commun.* **1998**, *1*, 7.
[5] H. C. Jewiss, W. Levason, M. Tajik, M. Webster, N. P. C. Walker, *J. Chem. Soc. Dalton Trans.* **1985**, 199.
[6] R. N. Mehrotra, R. C. Kapoor, S. K. Vajpai, *J. Chem. Soc. Dalton Trans.* **1984**, 999.
[7] S. Riedel, M. Kaupp, *Angew. Chem.* **2006**, *118*, 3791; *Angew. Chem. Int. Ed.* **2006**, *45*, 3708.
[8] X. Wang, L. Andrews, S. Riedel, M. Kaupp, *Angew. Chem.* **2007**, *119*, 8523; *Angew. Chem. Int. Ed.* **2007**, *46*, 8371.
[9] S. Riedel, M. Kaupp, *Coord. Chem. Rev.* **2009**, *253*, 606.
[10] F. Emich, *Monatsh. Chem.* **1908**, *29*, 1077.
[11] H. Schafer, H. J. Heitland, *Z. Anorg. Allg. Chem.* **1960**, *304*, 249.
[12] H. S. C. O'Neill, J. Nell, *Geochim. Cosmochim. Acta* **1997**, *61*, 5279.
[13] A. Citra, L. Andrews, *J. Phys. Chem. A* **1999**, *103*, 4182.
[14] G. J. Wang, M. F. Zhou, *Int. Rev. Phys. Chem.* **2008**, *27*, 1.
[15] Y. Gong, M. F. Zhou, *J. Phys. Chem. A* **2009**, *113*, 4990.
[16] a) M. E. Jacox, *Chem. Phys.* **1994**, *189*, 149; b) M. E. Jacox, *Chem. Soc. Rev.* **2002**, *31*, 108; c) M. E. Jacox, *Acc. Chem. Res.* **2004**, *37*, 727.
[17] C. J. Cramer, W. B. Tolman, K. H. Theopold, A. L. Rheingold, *Proc. Natl. Acad. Sci. USA* **2003**, *100*, 3635.
[18] H. A. O. Hill, D. G. Tew in *Comprehensive Coordination Chemistry*, *Vol. 2* (Eds.: G. Wilkinson, R. D. Gillard, J. A. McCleverty), Pergamon, Oxford, **1987**, p. 315.
[19] a) L. Vaska, *Acc. Chem. Res.* **1976**, *9*, 175; b) J. S. Valentine, *Chem. Rev.* **1973**, *73*, 235.
[20] Y. Gong, M. F. Zhou, L. Andrews, *J. Phys. Chem. A* **2007**, *111*, 12001.
[21] D. Danset, M. E. Alikhani, L. Manceron, *J. Phys. Chem. A* **2005**, *109*, 105.
[22] M. Zhou, A. Citra, B. Liang, L. Andrews, *J. Phys. Chem. A* **2000**, *104*, 3457.
[23] A. F. Holleman, E. Wiberg, *Lehrbuch der Anorganischen Chemie*, *Vol. 102*, Walter de Gruyter, Berlin, **2007**.
[24] Gaussian03 (Revision B.04 ed.), M. J. Frisch, G. W. Trucks, H. B. Schlegel, G. E. Scuseria, M. A. Robb, J. R. Cheeseman, J. A. Montgomery, J. T. Vreven, K. N. Kudin, J. C. Burant, J. M. Millam, S. S. Iyengar, J. Tomasi, V. Barone, B. Mennucci, M. Cossi, G. Scalmani, N. Rega, G. A. Petersson, H. Nakatsuji, M. Hada, M. Ehara, K. Toyota, R. Fukuda, J. Hasegawa, M. Ishida, T. Nakajima, Y. Honda, O. Kitao, H. Nakai, M. Klene, X. Li, J. E. Knox, H. P. Hratchian, J. B. Cross, C. Adamo, J. Jaramillo, R.

 © 2009 Wiley-VCH Verlag GmbH & Co. KGaA, Weinheim

Gomperts, R. E. Stratmann, O. Yazyev, A. J. Austin, R. Cammi, C. Pomelli, J. W. Ochterski, P. Y. Ayala, K. Morokuma, G. A. Voth, P. Salvador, J. J. Dannenberg, V. G. Zakrzewski, S. Dapprich, A. D. Daniels, M. C. Strain, O. Farkas, D. K. Malick, A. D. Rabuck, K. Raghavachari, J. B. Foresman, J. V. Ortiz, Q. Cui, A. G. Baboul, S. Clifford, J. Cioslowski, B. B. Stefanov, G. Liu, A. Liashenko, P. Piskorz, I. Komaromi, R. L. Martin, D. J. Fox, T. Keith, M. A. Al-Laham, C. Y. Peng, A. Nanayakkara, M. Challacombe, P. M. W. Gill, B. Johnson, W. Chen, M. W. Wong, C. Gonzalez, J. A. Pople, Pittsburgh PA, **2003**.

[25] A. D. Becke, *Phys. Rev. A* **1988**, *38*, 3098.

[26] J. P. Perdew, K. Burke, Y. Wang, *Phys. Rev. B* **1996**, *54*, 16533.

[27] A. D. Becke, *J. Chem. Phys.* **1993**, *98*, 5648.

[28] MOLPRO 2006.1 ed., H.-J. Werner, P. J. Knowles, R. Lindh, F. R. Manby, M. Schütz, P. Celani, T. Korona, G. Rauhut, R. D. Amos, A. Bernhardsson, A. Berning, D. L. Cooper, M. J. O. Deegan, A. J. Dobbyn, F. Eckert, C. Hampel, G. Hetzer, A. W. Lloyd, S. J. McNicholas, W. Meyer, M. E. Mura, A. Nicklaß, P. Palmieri, R. Pitzer, U. Schumann, H. Stoll, A. J. Stone, R. Tarroni, T. Thorsteinsson, Birmingham, UK, **2006**.

[29] D. Andrae, U. Häussermann, M. Dolg, H. Stoll, H. Preuss, *Theor. Chim. Acta* **1990**, *77*, 123.

[30] A. W. Ehlers, M. Bohme, S. Dapprich, A. Gobbi, A. Hollwarth, V. Jonas, K. F. Kohler, R. Stegmann, A. Veldkamp, G. Frenking, *Chem. Phys. Lett.* **1993**, *208*, 111.

[31] J. M. L. Martin, A. Sundermann, *J. Chem. Phys.* **2001**, *114*, 3408.

[32] T. H. Dunning, Jr., *J. Chem. Phys.* **1989**, *90*, 1007.

[33] S. Riedel, M. Straka, M. Kaupp, *Phys. Chem. Chem. Phys.* **2004**, *6*, 1122.

[34] S. Riedel, M. Kaupp, *Inorg. Chem.* **2006**, *45*, 1228.

[35] S. Riedel, M. Kaupp, *Inorg. Chem.* **2006**, *45*, 10497.

[36] M. Kaupp, M. Dolg, H. Stoll, H. G. von Schnering, *Inorg. Chem.* **1994**, *33*, 2122.

[37] W. Liu, C. van Wüllen, *J. Chem. Phys.* **1999**, *110*, 3730.

 © 2009 Wiley-VCH Verlag GmbH & Co. KGaA, Weinheim